Batteries & Supercaps

Research Article
doi.org/10.1002/batt.202400354

Chemistry Europe
European Chemical Societies Publishing

www.batteries-supercaps.org

Trace-Amount of Water as An Electrolyte Additive for Sodium Metal Electrode

Long Toan Trinh,[a] Thuan Ngoc Vo,*[a] and Il Tae Kim*[a]

The high reactivity of water toward Na metal has raised a concern about keeping the electrolytes extra-dried. In this work, changes in water concentration in electrolytes (with and without fluoroethylene carbonate) show changes in overpotential and the surface chemistry of Na electrodes. In a symmetric cell test, the cell with pristine electrolyte (1 M $NaClO_4$ in ethylene carbonate:propylene carbonate) sustained only 22 cycles before reaching the safety limit (5 V) at 1 mA cm^{-2}. Meanwhile, controlling the water content (40 ppm) extended the cell's life by 3.5 times. In fluoroethylene-carbonate-containing electrolytes, the optimized water concentration (40 ppm) gave the minimum overpotential (12 mV) after 170 cycles. Ex situ X-ray photoemission spectroscopy showed that water hydrolyzed fluoroethylene carbonate, which changed the Na electrode's surface chemistry. The appropriate amount of product (NaF) stabilized the electrodes' surfaces. Electrical impedance spectroscopy showed that the controlled traces amount of water (40 ppm) always gave the minimum values for resistances. For the pristine electrolytes, the resistances attributed to the charge-transfer process and the solid-electrolyte interface layer increased 51 times (from 45 Ω–2290 Ω) after cycling. Meanwhile, for the optimized sample, the resistances remarkably decreased by 93 % (from 264 Ω–19 Ω) after cycling.

Introduction

The depletion and high price of Li have prompted exploration of more sustainable alternatives to Li in energy storage systems. Due to the abundance of Na element and the similar chemical reactivity between Na and Li, sodium-ion batteries (SIBs) have emerged as a result of successful lithium-ion batteries (LIBs) implementation.[1–3] Both LIBs and SIBs share a common concern about prevention of dendrite growth on Li/Na metal electrodes' surfaces (counter electrodes).[4–6] As Li and Na are similar in chemical activity, SIBs can refer successful cases of dendrite prevention in LIBs.

In LIBs, dendrites cause several issues such as: (i) internal short-circuit, (ii) electrical isolation of active Li, and (iii) excessive solid-electrolyte interface (SEI) development.[7] The isolation of active Li led to a formation of discrete layers of inactive or "dead" Li. Accumulation of "dead" Li and SEI makes a cell's internal resistance continuously increase.[8,9] Furthermore, Li^+ ions have a significantly lower diffusivity in "dead" Li layers than in liquid electrolytes, which leads to a remarkable change in interfacial concentration of Li^+ ions throughout charge/discharge. That reduction on mass transport results in increasing of overpotential. A larger overpotential means a shorten in effective/actual working voltage for the related cell. Some materials are sensitive to changes in working voltage. For example, when the lower cut-off voltage increased 40 mV (from 60–100 mV), an Si anode lost 60 % of its 1st discharging capacity.[10] Likewise, SIBs also have materials that are sensitive to even minor changes in working voltage such as hard carbon.[11]

The complex behavior of metal anodes can be interpreted through voltage traces. Half-cycle voltage profiles of a symmetric cell usually have a "dendrite-bulk-pit" shape.[12,13] At the cathode, dendrite growth and nucleation are the two main processes. At the anode, they include dendrite dissolution, bulk dissolution, and pit formation. Overpotential increases with the consumption of dendrite and decreases with the formation of the pits. When the dominant reaction pathway moves to the bulk surface site, the cell's overpotential increases and peaks. Further dissolution of the bulk surface expands the active area and form pits, which results in a decrease of overpotential.

Using electrolyte additives is an effective, convenient strategy on suppressing dendrites, reducing overpotential, and enhancing the metal counter electrodes' performances. J. Zhong et al. introduced an ionic liquid (Pyr1(10)TFSI) as a non-consuming electrolyte additive allowing uniform metal deposition via an electrostatic shielding mechanism.[14] At 1 mA cm^{-2}, the overpotential of the adjusted electrolyte was 8.9 mV after 100 cycles, whereas that of the blank one was 10.5 mV. Meanwhiles, J. Qian et al. used trace-amounts of water (25–50 ppm) as an electrolyte additive in LIBs and created LiF-rich SEI layers via the decomposition of $LiPF_6$ on Li metal foil.[15] In SIBs, M. Xu fabricated NaF-rich SEI layers via a reaction between molten Na metal and poly(tetrafluoroethylene) for inhibiting Na dendrites.[16] The NaF-protected electrode exhibited a small overpotential of 8 mV. In facts, fluoroethylene carbonate (FEC) is usually introduced to $NaClO_4$-based electrolytes to deposit NaF on electrodes' surface.[17] The addition of FEC is essential because conventional $NaClO_4$-based electrolytes lack of the ability of forming stable SEI layers.[18]

[a] L. T. Trinh, T. N. Vo, I. T. Kim
Department of Chemical, Biological and Battery Engineering, Gachon University, 1342 Seongnam-daero, Sujeong-gu, Seongnam-si, Gyeonggi-do 13120, South Korea
E-mail: vnthuanbk@gmail.com
itkim@gachon.ac.kr

Supporting information for this article is available on the WWW under https://doi.org/10.1002/batt.202400354

In this study, trace-amount of water was introduced as an effective electrolyte additive for SIBs. When using FEC as the only additive, the overpotential was still large (0.1–0.35 V). The addition of water accelerated and fastened FEC's decomposition, which effectively kept the overpotential at 10–16 mV. Ex-situ x-ray photoemission spectroscopy (XPS) and electrochemical impedance spectroscopy (EIS) analysis suggested that an appropriate amount of NaF within SEI layers was the key to achieving a low overpotential and stabilizing Na metal electrodes.

Results and Discussion

Figures 1a–c shows the effect of water content on the voltage hysteresis of Na symmetric cell. Generally, the overpotential increased by cycling times. For the pristine electrolyte, the overpotential in the first cycle could be up to 0.39 V, as shown in Figure 1a. It started a drastic increase after 35 h of operation before stopping at the 48th hour due to safety limit (5 V). Meanwhile, in Figure 1b, the overpotential of the cell having a water content of 40 ppm was up to 0.41 V in the first cycle and reached the safety limit at after 160 h, which was 4.6 times that of the pristine electrolyte. Increasing the water content to 100 ppm worsened the performance, as a spike existed in the 23rd h (Figure 1c). The aforementioned spike raises a safety concern and might be correlated with gas evolution due to water contamination. The peaking voltage profiles in half-cycles were typical for a conventional symmetric cell with three stages governing mainly at the anode: (i) the overpotential increased with the dissolution of dendrites, (ii) the overpotential peaked at around the complete depletion of active dendrites, and (iii) pits formed with the decrease in overpotential. The peaking profiles indicated continuous development of dendrite over cycling.[13]

Figure 1d shows the response of overpotential to the variation of current density. Overall, the overpotential was proportional to the current density. A higher current density usually fastens the degradation of a metal electrode via accelerating dendrite growth and creating more dead parts. When the water content was 40 ppm, the overpotential at 0.5, 1, 2, 5, 10, and 20 mA cm^{-2} were 0.15, 0.15, 0.21, 0.43, and 0.59 V, respectively. Meanwhile, the pristine sample and the "100 ppm" one were unable to finish the test due to their rapid degradation from 5 mA cm^{-2}.

Figures 2a–c shows the effect of water content on the voltage hysteresis of Na symmetric cell with the presence of FEC. For the pristine electrolyte, the overpotential in the first cycle could be up to 0.77 V, as shown in Figure 2a. Remarkably, the voltage profile suddenly changed its shape from a dendrite-bulk-pit shape to a square one in the 21st h. The period from the 4th h–the 21st h is referred to as an activation period. The square shape of the voltage profile usually indicates uniform kinetics across the surface of an electrode via suppressing

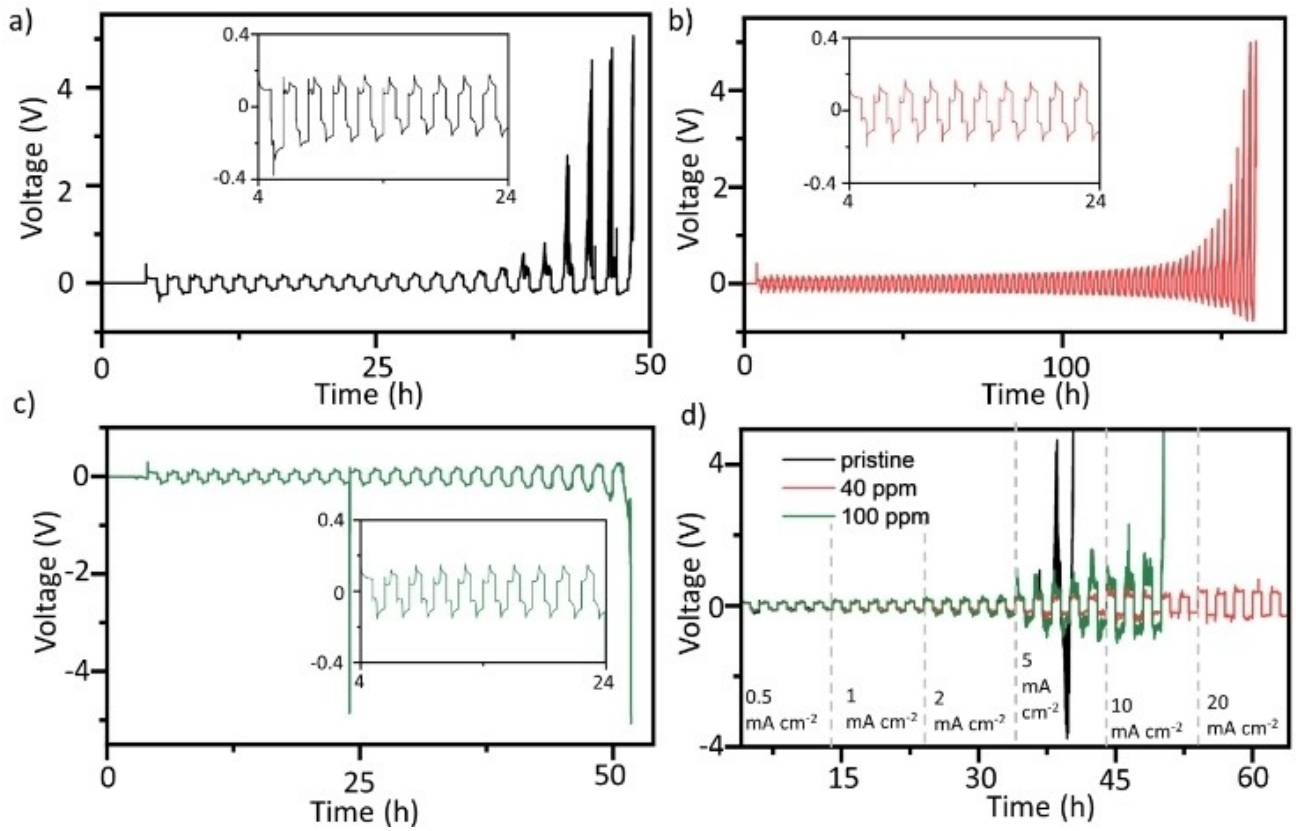

Figure 1. Voltage profiles of Na symmetric cells made with 1 M $NaClO_4$ in EC:PC at various additional water concentration: (a) pristine (no additional water), (b) 40 ppm, and (c) 100 ppm at 1 mA cm^{-2}; (d) voltage profiles of the Na symmetric cells at different current densities.

Research Article
doi.org/10.1002/batt.202400354
Chemistry Europe
European Chemical Societies Publishing

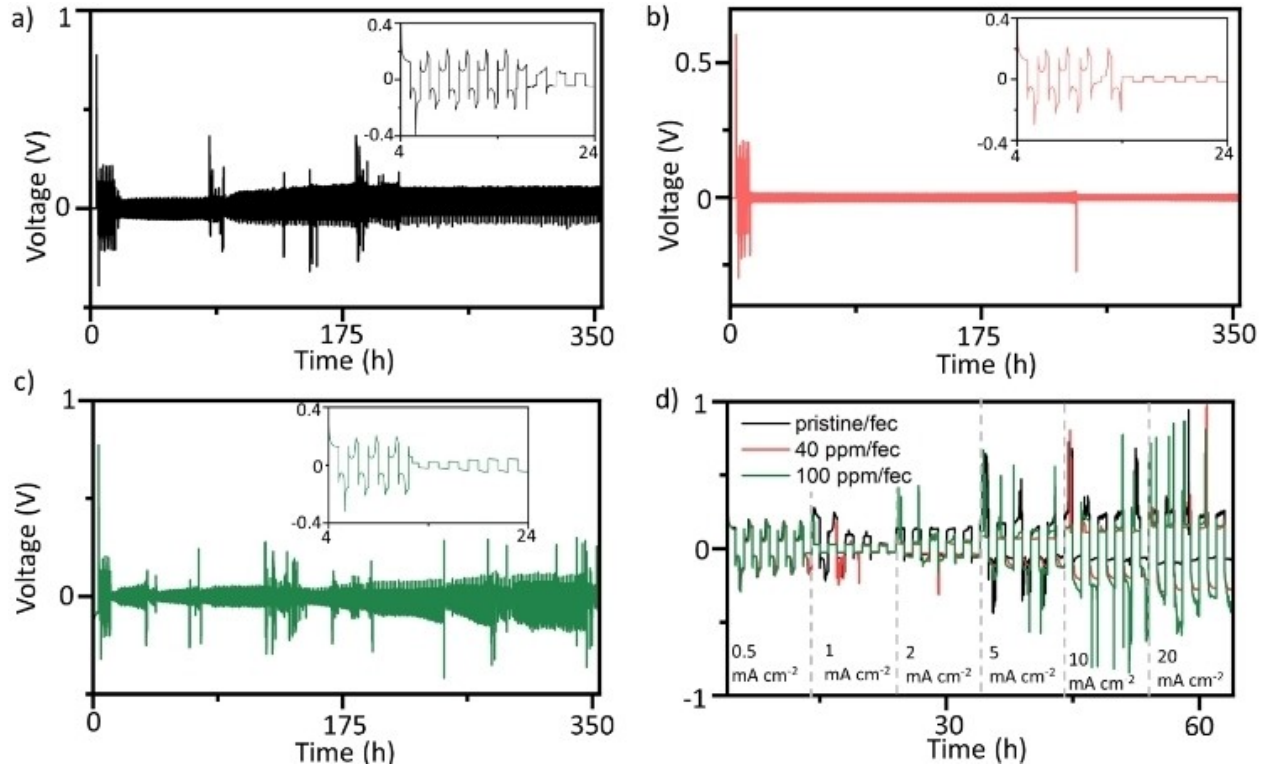

Figure 2. Voltage profiles of Na symmetric cells made with 1 M $NaClO_4$ in EC:PC:FEC at various additional water concentration: (a) pristine (no additional water), (b) 40 ppm, and (c) 100 ppm at 1 mA cm^{-2}; (d) voltage profiles of the Na symmetric cells at different current densities.

dendrite growth.[13,19] The activation period might be related to the decomposition of FEC, forming a stable SEI layer, as the samples without FEC did not exhibit similar behavior (Figure 1a). For the "pristine/fec" sample, the accumulated capacity for the activation period and the over potential right after the activation period were 17 mAh cm^{-2} and 45 mV, respectively. The activation period signifies that a fresh Na metal electrode still face a considerably large overpotential even in the presence of FEC, until the activation period finishes. A long activation period is not preferred, because a working electrode with low areal capacity may not finish the activation period within a short cycling test time. In the 355th h, the overpotential was 68 mV. Regarding the "40 ppm/fec" sample, the initial overpotential was 0.6 V, as shown in Figure 2b. The activation period lasted until the 14th h, which was 7 h sooner than that of the "pristine/fec" sample. The accumulated capacity for the activation period and the over potential right after the activation period were 10 mAh cm^{-2} and 18 mV, respectively. In the 355th h, the overpotential was 12 mV. Further increasing the water content shortened the activation period. Namely, the activation period in the "100 ppm/fec" sample was until the 13th h, which was 1 h sooner than that of the "40 ppm/fec" sample (Figure 2c). That shortening of the activation period suggests that the water contamination accelerated the decomposition of FEC on the Na electrode. However, the overpotential of the "100 ppm/fec" sample in the 355th h was the largest (255 mV) among FEC-contaminated samples.

Figure 2d shows the response of overpotential to the variation of current density with the presence of FEC. Overall, the voltage profiles became "noisier" when the current density suddenly increased, which was different from the FEC-free samples (Figure 1d). Namely, a significant of overpotential enlargement occurred right after an increase in capacity density. The SEI layers created during the activation period at a lower current density might be insufficient at a higher current density. By excluding the overpotential right after increasing the current density, for the "40 ppm/fec" sample, the overpotential at 1, 2, 5, 10, and 20 mA cm^{-2} were 0.021, 0.032, 0.12, 0.2, and 0.98 V, respectively. Meanwhile, the corresponding values for the "100 ppm/fec" sample were 0.028, 0.16, 0.57, 0.81, and 0.87 V. In the range of current density from 1–10 mA cm^{-2}, the "40 ppm/fec" sample exhibited the smallest overpotential among the samples. Generally, higher current densities facilitate the growth of dendrite recognized through the peaking voltage profiles.[20] Although the introduced SEI layers can stabilize the surface, a high-enough current density can defeat the protecting layers and develop dendrites. In Figures 2d, 5 mA cm^{-2} seemed to be the critical current density, because the peaking voltage profile appears.

Figure 3 summarizes the overpotential of the symmetric cells made from various electrolytes over cycles. Irrespective of FEC, the electrolytes with trace amount of water (40 ppm) showed the highest performance. The sharp inclines observed in the overpotential suggest that potential failures in half-cell tests primarily stem from the counter electrode (Na metal)

Research Article
doi.org/10.1002/batt.202400354
Chemistry Europe
European Chemical Societies Publishing

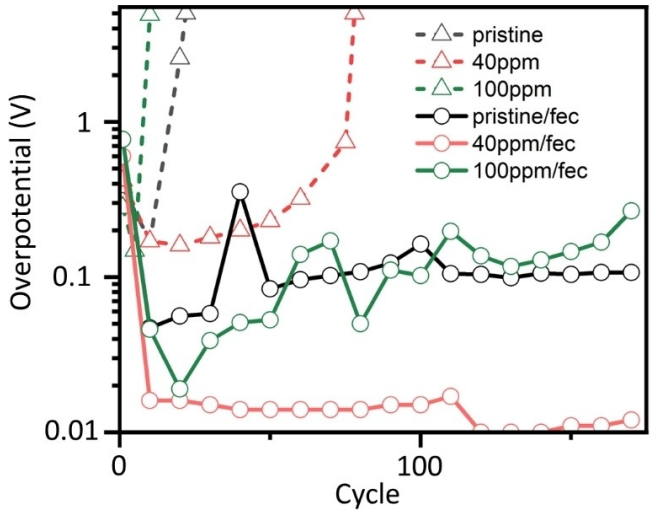

Figure 3. Overpotential of Na symmetric cells made with various electrolyte by cycle at 1 mA cm^{-2}.

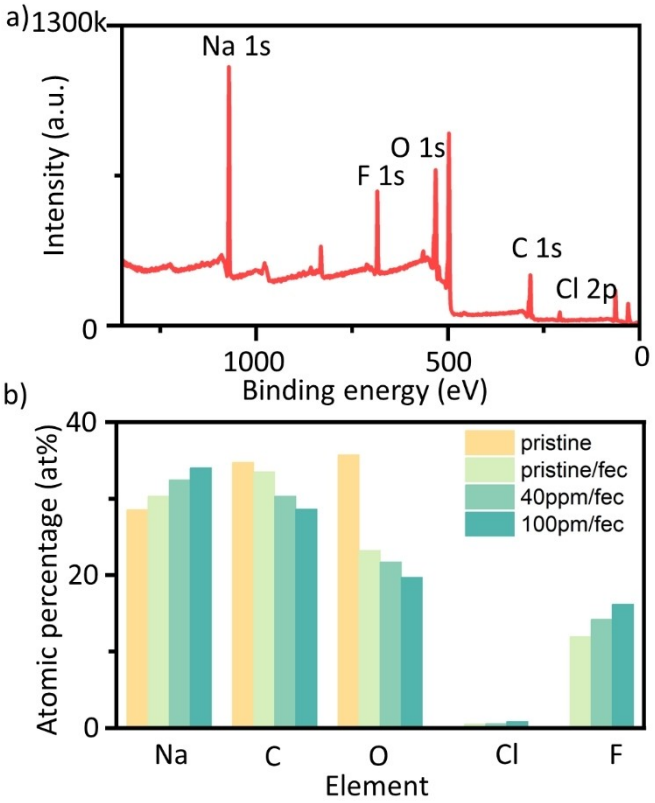

Figure 4. Ex situ XPS analysis of cycled Na metal electrodes: (a) survey scan for the "40 ppm/fec" sample, and (b) elemental concentration by sample.

rather than the working electrode for the FEC-free electrolytes. Despite the improvement in performance with the addition of FEC, the overpotential starting from the 40th cycle remained too large (0.1–0.35 V), posing challenges for characterizing materials operated at low potential such as hard carbon. By adding a trace amount of water to the FEC-containing electrolyte, the overpotential was stabilized at 10–16 mV, which represents an improvement of 3–25 times compared to the "pristine/fec" sample, from the 10th–the 170th cycle. Unlike the other FEC-containing samples, the overpotential of the "100 ppm/fec" sample continuously increased with the number of cycles. It approached the levels of "40 ppm/fec" sample in the initial cycles and surpassed the "pristine/fec" sample from the 60th cycle onward.

Figure 4 reveals the elemental diversity of the Na metal electrodes after cycling via ex situ XPS characterization. Typically, for the FEC-containing samples, all the cycled Na electrodes' surfaces contained C (284.44 eV), Cl (198.09 eV), F (683.79 eV), O (530.98 eV), and Na (1070.86 eV) (Figure 4a). However, their contents varied with the amount of water added. Overall, by adding water, C and O decreased, whereas F increased (Figure 4b). The Na : C : O:(F + Cl) ratios in the "pristine/fec", "40 ppm/fec", and "100 ppm/fec" were 1 : 1.1 : 0.77 : 0.41, 1 : 0.93 : 0.67 : 0.45, and 1 : 0.84 : 0.58 : 0.5, respectively. Besides, the Na electrode's surface for the "pristine" sample was noticeably rich in O, which suggests a considerable difference at the SEI layer between the FEC-free and the FEC-containing samples.

Figure 5 provides detail information about Na1s, C1s, Cl2p, and F1s on the surfaces of Na electrodes in the "pristine", "pristine/fec", "40 ppm/fec", and "100 ppm/fec" samples. In Figure 5a, all the spectra peak at 1070.8–1070.9 eV corresponding to Na salts. The addition of water in the preparation of the "40 ppm/fec" and the "100 ppm/fec" raised concerns on the reaction between Na metal and water, which would lead to the formation of NaOH. However, because all the spectra are similar and do not show signals at 1072.6 eV (NaOH), the aforementioned reaction seemed not to be happening. Regarding C1s (Figure 5b), typical components involve C–C (284.4 eV), C–O–C (286.0 eV), O–C=O (288.0 eV), and OCOO (289.2 eV). Compared to the "pristine" sample, the FEC-containing samples exhibit a decrease in carbonate (OCOO) and an increase in organic species (C–C and C–O–C), which means FEC significantly changed the SEI's components. Deconvolution of Cl2p suggests that all the FEC-containing electrolytes delivered ClO_4^- (208.1 eV) and some decomposition products (NaCl (198.0 eV) and ClO_3^- (206.1 eV)) on the electrodes' surfaces. However, the "pristine" sample does not give any signal of Cl2p within the observation range (210–195 eV), which means that ClO_4^- did not participated in the formation of SEI from the "pristine" electrolyte. Besides, because the amount of NaCl was proportional to the added amount of water, water contributed to the decomposition of ClO_4^-. The Na : Cl molar ratios in the "pristine/fec", "40 ppm/fec", and "100 ppm/fec" samples were 1:0.017, 1:0.017, and 1:0.025 mol/mol, respectively. Those ratios suggests that the decomposition of ClO_4^- to form the SEI layers was minor. Figure 5d shows the presence of F in the form of NaF (683.8 eV) in all the FEC-containing samples. The absence of peaks from 689–686 eV in all the spectra indicates that organic F was not present on the Na electrodes' surfaces.

Accordingly, the "pristine" electrolyte developed an SEI layer containing Na_2CO_3 and some organic species. In contrast, FEC altered the SEI layer, resulting in less Na_2CO_3 and more organic species. FEC decomposed into NaF itself; it also catalysed the

Research Article
doi.org/10.1002/batt.202400354
Chemistry Europe
European Chemical Societies Publishing

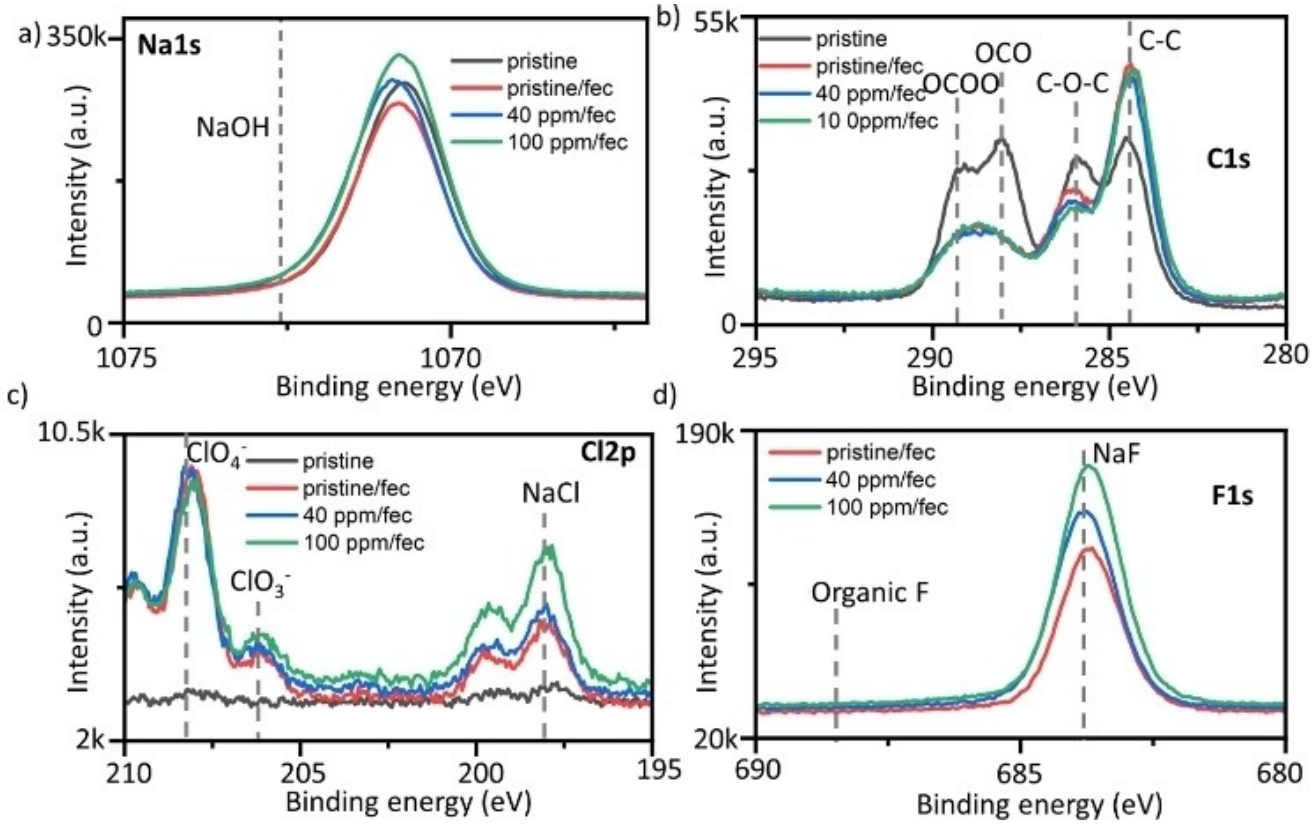

Figure 5. Ex situ XPS analysis of Na electrodes cycled in various electrolytes (pristine, pristine/fec, 40 ppm/fec, 100 ppm/fec): (a) Na1s, (b) C1s, (c) Cl2p, and (d) F1s.

decomposition of $NaClO_4$ (minor). Water facilitated the decomposition of FEC into NaF, as the NaF content increased by adding more water. Within the observation ranges ($H_2O <$ 100 ppm), the decomposition of FEC was more favoured than the Na-water reaction, because NaOH was not observed in any of the spectra.

Figure 6 presents the EIS results of typical samples by cycles. Overall, the impedance of the FEC-free samples increased with the cycling time, whereas that of the FEC-containing sample dropped by cycling time. To interpret EIS, an electrical involve three resistors and two constant-phase elements (CPEs) was employed (Figure 7a).[21] The three resistors describe series (R_s), charge-transfer (R_{ct}), and SEI layer's resistance (R_{SEI}). The two CPEs describe the imperfect capacitive effects of the charge-transfer process (CPE_1) and the SEI layer (CPE_2). Compared to a conventional Na half-cell, an Na symmetric cell does not have an element describing diffusion because Na^+ ion does not need to diffuse into the inner structure of the host material. The impedance of CPE_1 and CPE_2 depends on the applied frequency ω:[22]

$$Z_{CPE1} = \frac{1}{A(\omega i)^{\alpha}},\ 0.5 < \alpha < 1 \tag{1}$$

$$Z_{CPE2} = \frac{1}{B(\omega i)^{\beta}},\ 0.5 < \beta < 1 \tag{2}$$

Total impedance of the circuit is:

$$Z = R_s + Z_1 + Z_2 \tag{3}$$

$$Z_1 = \frac{R_{ct} \times Z_{CPE1}}{R_{ct} + Z_{CPE1}} = \frac{R_{ct}}{AR_{ct}(\omega i)^{\alpha} + 1} = \frac{R_{ct}}{1 + AR_{ct}\omega^{\alpha}(\cos\frac{\pi\alpha}{2} + \mathrm{i} \times \sin\frac{\pi\alpha}{2})} \tag{4}$$

Call ψ as the denominator of the above equation, its complex conjugate is:

$$\overline{\psi} = 1 + AR_{ct}\omega^{\alpha}\cos\frac{\pi\alpha}{2} - AR_{ct}\omega^{\alpha}\sin\frac{\pi\alpha}{2} \times i \tag{5}$$

$$|\psi|^2 = 1 + A^2R_{ct}^2\omega^{2\alpha} + 2AR_{ct}\omega^{\alpha}\cos\frac{\pi\alpha}{2} \tag{6}$$

$$Z_1 = \frac{R_{ct}\overline{\psi}}{|\psi|^2} = \frac{R_{ct}(1 + AR_{ct}\omega^{\alpha}\cos\frac{\pi\alpha}{2} - AR_{ct}\omega^{\alpha}\sin\frac{\pi\alpha}{2} \times i)}{|\psi|^2} \tag{7}$$

When ω approaches 0, ω^{α} and $\omega^{2\alpha}$ also approach 0:

$$\lim_{\omega \to 0} |\psi|^2 = 1 \tag{8}$$

Research Article
doi.org/10.1002/batt.202400354
Chemistry Europe
European Chemical Societies Publishing

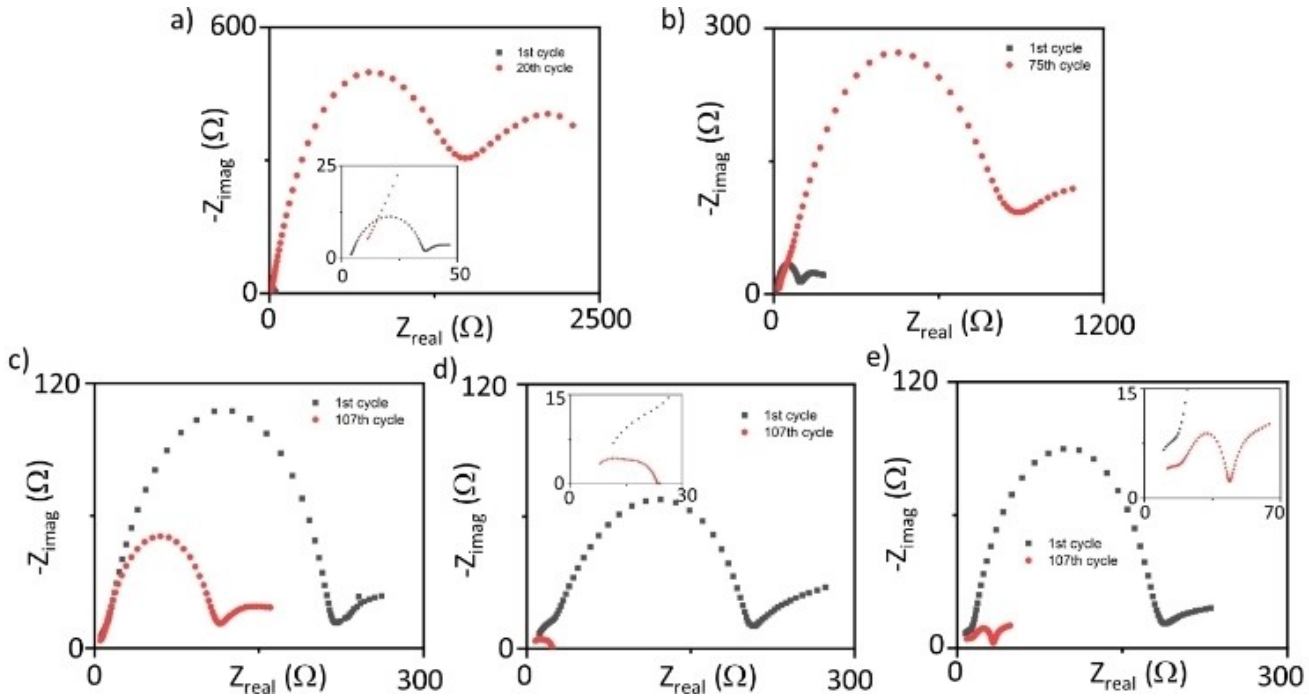

Figure 6. EIS analysis of Na symmetric cells made with various electrolytes: (a) pristine, (b) 40 ppm, (c) pristine/fec, (d) 40 ppm/fec, and (e) 100 ppm/fec.

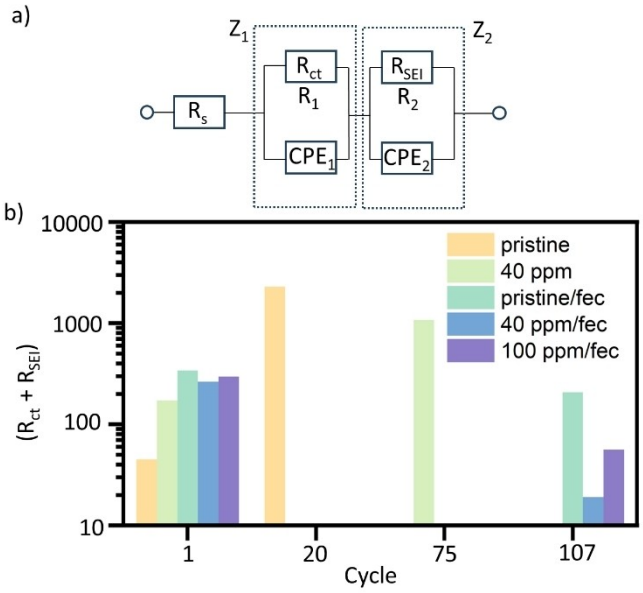

Figure 7. (a) Equivalent circuit and (b) refined ($R_{ct}+R_{SEI}$) for Na symmetric cell made with various electrolytes.

$$\lim_{\omega\to 0} Z_1 = R_{ct} \tag{9}$$

By performing the similar approximation for the 2nd subcircuit:

$$\lim_{\omega\to 0} Z_2 = R_{SEI} \tag{10}$$

$$\lim_{\omega\to 0} Z = R_s + R_{ct} + R_{SEI} \tag{11}$$

According to (11), for the specified circuit, the total resistance ($R_s+R_{ct}+R_{SEI}$) is the interception between the impedance and the x-axis in the Nyquist plot. However, actual EIS curves rarely cut the x-axis in a Nyquist plot. To prevent overfitting during extrapolation, the sum of ($R_s+R_{ct}+R_{SEI}$) is approximated to be equal to the real part of impedance at the lowest frequency (as ω approaches 0). The approximation is more accurate when the imaginary part of the selected impedance also approaches 0. Besides, (3) does not allow distinguishing R_{ct} and R_{SEI}, as Z_1 and Z_2 are mathematically equivalent. Usually, uncertainty of Rs regression is negligible, so the sum of ($R_{ct}+R_{SEI}$), which is approximately the difference between the real part of impedance at the lowest frequency (as ω approaches 0) and R_s obtained via numerical methods, seems more reasonable when comparing and interpreting EIS results for the specified circuit (Figure 7a).

Table 1 presents the interpretation of EIS spectra via a numerical method (ZMAN 2.5).[22,23] The numerical method can return regressed parameters with large uncertainties. For example, the uncertainty in regressing R_2 for the "pristine" sample after the 1st cycle is 5×10^{12} Ω. However, the numerical regression for the "40 ppm/fec" sample after 107th cycle was reasonable, as the uncertainties, residual of |Z|, and delta phase are minor. The sum of ($R_s+R_1+R_2$) was 23.8 Ω, which is 0.7% smaller than the real part of the impedance at 100 mHz (23.96 Ω). The small difference suggests that the approximation (11) can be applied to retrieve ($R_{ct}+R_{SEI}$) for the other samples. Employing the sum of ($R_{ct}+R_{SEI}$) (=R_1+R_2) is more useful than

Research Article
doi.org/10.1002/batt.202400354
Chemistry Europe
European Chemical Societies Publishing

Table 1. Simulated parameters obtained from a numerical method (complex nonlinear least-squares analysis).

Sample		Rs [Ω]	R_1 [Ω]	R_2 [Ω]	Residual of $\|Z\|$ [a] [%]	Delta phase [b] [degree]
Pristine	1st cycle	1.6 ± 0.7	27 ± 2	$10^7 \pm 5\times10^{12}$	−2 ÷ 4	−2 ÷ 1
	20th cycle	5.6 ± 6.9	$2.5\times10^3 \pm 6.6\times10^3$	1092 ± 848	−2 ÷ 6	−0.1 ÷ 2
40 ppm	1st cycle	7.8 ± 0.4	98 ± 47	86 ± 11	−2 ÷ 7	−4 ÷ 2
	75th cycle	16.7 ± 9.0	975 ± 289	107 ± 792	−8 ÷ 8	−5 ÷ 4.5
Pristine/fec	1st cycle	7.7 ± 3.0	35 ± 166	304 ± 43	−9 ÷ 11	−14 ÷ 5
	107th cycle	6.9 ± 1.3	48 ± 59	155 ± 18	−7 ÷ 8	−12 ÷ 4
40 ppm/fec	1st cycle	9.4 ± 5.5	221 ± 43	44 ± 154	−10 ÷ 11	−11 ÷ 6
	107th cycle	4.8 ± 0.9	8 ± 4	11 ± 3	−0.8 ÷ 2	−0.4 ÷ 0.3
100 ppm/fec	1st cycle	11 ± 3.4	254 ± 40	33 ± 129	−10 ÷ 18	−22 ÷ 7
	107th cycle	8.1 ± 3.1	42 ± 8	22 ± 19	−5 ÷ 6	−6 ÷ 3

[a] Residue of $|Z|$: the relative difference between the magnitude of the actual and the simulated Z (via numerical method). For an ideal simulation, it approaches 0. [b] Delta phase: the difference between the argument of the actual and the simulated Z (via numerical method). For an ideal simulation, it approaches 0.

separating R_{ct} and R_{SEI} because R_{ct} and R_{SEI} are indistinguishable in the selected model (R_{ct} can be either R_1 or R_2, and vice versa).

Figure 7b presents $(R_{ct}+R_{SEI})$ of the samples via combining (11) and Table 1. Overall, $(R_{ct}+R_{SEI})$ rapidly increased in the cycled FEC-free samples, whereas it considerably decreased in the cycled FEC-containing ones. In FEC-free samples, accumulation of dead "Na" metal and continuously growth of SEI layers might lead to the aforementioned increase in $(R_{ct}+R_{SEI})$. The rate of increasing $(R_{ct}+R_{SEI})$ for the "pristine" sample was the fastest (from 45 Ω–2290 Ω after 20 cycles), which results in the shortest lifespan of the "pristine" sample. Meanwhiles, the FEC-containing electrolytes created NaF-rich SEI layers facilitating the plating/striping of Na^+ ions, especially after the activation period, so $(R_{ct}+R_{SEI})$ decreased. The values of $(R_{ct}+R_{SEI})$ for the "pristine/fec", "40 ppm/fec", and "100 ppm/fec" samples after the 1st cycle were 341, 264, and 296 Ω, respectively. After 107 cycles, the dropping rate $(R_{ct}+R_{SEI})$ for the "pristine/fec", "40 ppm/fec", and "100 ppm/fec" samples were 39%, 93%, and 81%, respectively. Accordingly, the NaF content in the "pristine/fec" sample was insufficient to cause a drastic drop in $(R_{ct}+R_{SEI})$, whereas the SEI layers in the "100 ppm/fec" sample with excessive NaF resisted the drop in $(R_{ct}+R_{SEI})$ (Figure 6d). The appropriate NaF amount created by adding the trace amount of water (40 ppm) to the FEC-containing electrolyte was sufficient to give the minimum $(R_{ct}+R_{SEI})$.

Compared to the 40 ppm sample, EIS results (Figure 7b) suggest that the SEI layers in the 100 ppm samples cause a significant increase in $Rct+R_{SEI}$. In Figure 2d, above the critical current density, the accumulation of dead Na dendrites (as a part of a typical peaking voltage profile) including SEI layers on their surfaces would accelerate the increase of overpotential exponentially. Therefore, the difference in overpotential by gradient concentration among samples were more severe at higher current densities.

Conclusions

At trace amounts, water can serve as a potential electrolyte additive for stabilizing Na metal electrode, particularly when used in conjunction with FEC. FEC compensated for the high stability of $NaClO_4$ by forming NaF-rich SEI layers, a process that required a certain period. After completing the activation period, the voltage profile changed to a square shape proving dendrite growth suppression. Water facilitated the decomposition of FEC on Na metal electrodes' surfaces, as adding more water shortened the activation period. An appropriate amount of water (40 ppm) minimized the overpotential of Na metal plating/stripping via controlling the presence of NaF (an FEC decomposition product) at a suitable level within the SEI layers. Higher concentrations of water were detrimental to the electrochemical performance. Besides, water preferred to decompose FEC rather than attack on Na metal, as evidenced in the ex situ XPS analysis. Regarding EIS analysis, total resistances attributed to the charge-transfer process and the SEI layers $(R_{ct}+R_{SEI})$ increased over cycling time for the FEC-free samples, whereas that of the FEC-containing samples decreased due to the presence of NaF. The rate of reduction in $(R_{ct}+R_{SEI})$ depended on the NaF content of the SEI layers. At the optimum point, where a trace amount of water was added (40 ppm), the decline reached its maximum magnitude.

Experimental Section

Symmetric cells (CR 2032-coin) were assembled in an Ar-filled glove box. The working and the counter electrodes were Na metal (Sigma, 99.9%). Glass fiber was the separator. To prepare the pristine electrolyte, 1.22 g of $NaClO_4$ (Sigma, 98%) was dissolved in 10 ml of solvent (ethylene carbonate (Sigma, 99%, $H_2O < 10$ ppm) (EC): propylene carbonate (Sigma, 99,7%, anhydrous) (PC) 1:1 v/v). Water concentration was adjusted by added deionized water into the solvent in prior to Karl Fischer titration. For FEC-contaminated

electrolytes, FEC (Sigma, 99%), which was added after the water adjustment step, shared 10% of the volume of the solvent.

A Karl Fischer coulometric titrator (Mettler Toledo, C10s, without diaphragm) using an anolyte coulometric reagent (Honeywell, Hydranal – Coulomat AG) was employed for water quantification. To characterize the surface chemistry of Na electrodes after cycling, the cells were disassembled for ex situ XPS (Nexsa V2, Al Kα) examination. The collected Na electrodes were washed several times with dimethyl carbonate and attached to Si wafers. To avoid impurities caused by reactions between the as-prepared Na electrodes and the air, all the steps related to the ex situ XPS characterization (sample preparation, transfer, and measurement) were carried out under Argon atmosphere.

For cycling characterization, after a resting time of 4 hours, the symmetric cell was discharged and charged at a current density of 1 mA cm^{-2} to reach an areal capacity of 1 mAh cm^{-2}. The cycling tests were performed on an automatic battery cycler system (WBCS3000, WonATech). EIS analysis was carried out from 100 kHz–100 mHz on a ZIVE MP1 station (WonATech).

Acknowledgements

This study was supported by a National Research Foundation of Korea (NRF) grant funded by the Korean government (MSIT) (NRF-2022R1F1A1062928). This research was also supported by the Basic Science Research Capacity Enhancement Project through a Korea Basic Science Institute (National Research Facilities and Equipment Center) grant funded by the Ministry of Education (2019R1A6C1010016).

Conflict of Interests

The authors declare no conflict of interest.

Data Availability Statement

The authors declare that the data supporting the findings of this study are available within the paper and the Supplementary Information file.

Keywords: Sodium metal electrode · Overpotential · Symmetric cell · Ex situ XPS · Water additive

[1] I. T. Kim, E. Allcorn, A. Manthiram, *Phys. Chem. Chem. Phys.* **2014**, *16* (25), 12884–12889.
[2] I. T. Kim, S. O. Kim, A. Manthiram, *J. Power Sources* **2014**, *269*, 848–854.
[3] S. Chen, L. P. Lv, S. Xiao, W. Sun, X. Li, Y. Wang, *Ind. Eng. Chem. Res.* **2018**, *57* (29), 9420–9429.
[4] X. Liu, X. Lei, Y. G. Wang, Y. Ding, *ACS Cent. Sci.* **2021**, *7*(2), 335–344.
[5] D. Tewari, S. P. Rangarajan, P. B. Balbuena, Y. Barsukov, P. P. Mukherjee, *J. Phys. Chem. C* **2020**, *124* (12), 6502–6511.
[6] M. Zhu, G. Wang, X. Liu, B. Guo, G. Xu, Z. Huang, M. Wu, H. K. Liu, S. X. Dou, C. Wu, *Angew. Chem. Int. Ed.* **2020**, *59* (16), 6596–6600.
[7] K. H. Chen, K. N. Wood, E. Kazyak, W. S. Lepage, A. L. Davis, A. J. Sanchez, N. P. Dasgupta, *J. Mater. Chem. A Mater.* **2017**, *5* (23), 11671–11681.
[8] Y. Zhao, Y. Wu, H. Liu, S. L. Chen, S. H. Bo, *ACS Appl. Mater. Interfaces* **2021**, *13* (30), 35750–35758.
[9] U. Janakiraman, T. R. Garrick, M. E. Fortier, *J. Electrochem. Soc.* **2020**, *167* (16), 160552.
[10] A. Tornheim, S. E. Trask, Z. Zhang, *J. Electrochem. Soc.* **2019**, *166* (2), A132–A134.
[11] X. Chen, Y. Zheng, W. Liu, C. Zhang, S. Li, J. Li, *Nanoscale* **2019**, *11* (46), 22196–22205.
[12] Y. Feng, C. Zhang, B. Li, S. Xiong, J. Song, *J. Mater. Chem. A Mater.* **2019**, *7*(11), 6090–6098.
[13] K. N. Wood, E. Kazyak, A. F. Chadwick, K. H. Chen, J. G. Zhang, K. Thornton, N. P. Dasgupta, *ACS Cent. Sci.* **2016**, *2*(11), 790–801.
[14] J. Zhong, Z. Wang, S. Wang, X. Li, H. Guo, J. Wang, G. Yan, *Appl. Surf. Sci.* **2023**, *622*, 156968.
[15] J. Qian, W. Xu, P. Bhattacharya, M. Engelhard, W. A. Henderson, Y. Zhang, J. G. Zhang, *Nano Energy* **2015**, *15*, 135–144.
[16] M. Xu, Y. Li, M. Ihsan-Ul-Haq, N. Mubarak, Z. Liu, J. Wu, Z. Luo, J. K. Kim, *Energy Storage Mater.* **2022**, *44*, 477–486.
[17] J. Park, K. Ku, S.-B. Son, J. Gim, Y. Kim, E. Lee, C. Johnson, *J. Electrochem. Soc.* **2022**, *169* (3), 030536.
[18] U. Purushotham, N. Takenaka, M. Nagaoka, *RSC Adv.* **2016**, *6* (69), 65232–65242.
[19] D. Wang, F. Zhang, P. He, H. Zhou, *Angew. Chem. Int. Ed.* **2019**, *58* (8), 2355–2359.
[20] J.-F. Ding, Y.-T. Zhang, R. Xu, R. Zhang, Y. Xiao, S. Zhang, C.-X. Bi, C. Tang, R. Xiang, H. S. Park, Q. Zhang, J.-Q. Huang, *Green Energy & Environ.* **2023**, *8* (6), 1509–1530.
[21] J. Hwang, K. Matsumoto, R. Hagiwara, *J. Phys. Chem. C* **2018**, *122* (47), 26857–26864.
[22] T. N. Vo, D. S. Kim, Y. S. Mun, H. J. Lee, S. Ahn, I. T. Kim, *Chem. Eng. J.* **2020**, *398*, 125703.
[23] J. Son, T. N. Vo, S. Cho, A. N. Preman, I. T. Kim, S. Ahn, *J. Power Sources* **2020**, *458*, 228054.

Manuscript received: May 30, 2024
Revised manuscript received: August 26, 2024
Accepted manuscript online: September 10, 2024
Version of record online: October 28, 2024